Enhancing the efficiency of slit-coupling to surface-plasmon-polaritons via dispersion engineering

R. Mehfuz, M. W. Maqsood, and K. J. Chau

School of Engineering, University of British Columbia Okanagan, 3333 University Way, Kelowna, BC V1V1V7

kenneth.chau@ubc.ca

Abstract: We describe a simple method for enhancing the efficiency of coupling from a free-space transverse-magnetic (TM) plane-wave mode into a surface-plasmon-polariton (SPP) mode. The coupling structure consists a metal film with a dielectric-filled slit and a planar, dielectric layer on the slit-exit side of the metal film. By varying the dielectric layer thickness, the wavevector of the SPP mode on the metal surface can be tuned to match the wavevector magnitude of the modes emanating from the slit exit, enabling high-efficiency radiation coupling into the SPP mode at the slit exit. An optimal dielectric layer thickness $\simeq 100\,\text{nm}$ yields a visible-frequency SPP coupling efficiency $\simeq 4$ times greater than the SPP coupling efficiency without the dielectric layer. Commensurate coupling enhancement is observed spanning the regime $400\,\text{nm} \leq \lambda_0 \leq 700\,\text{nm}$. We map the dependence of the SPP coupling efficiency on the slit width, the dielectric-layer thickness, and the incident wavelength to fully characterize this SPP coupling methodology.

OCIS codes: (240.6680),(350.4600)

References and links

1. S. A. Maier, M. L. Brongersma, P. G. Kik, S. Meltzer, A. A. G. Requicha, and H. A. Atwater, "Plasmonics - a route to nanoscale optical devices," Adv. Mater. **13**, 1501–1505 (2001).
2. T. Nikolajsen, K. Leosson, I. Salakhutdinov, and S. I. Bozhevolnyi, "Polymer-based surface-plasmon-polariton stripe waveguides at telecommunication wavelengths," Appl. Phys. Lett. **82**, 668–670 (2003).
3. R. Charbonneau, N. Lahoud, G. Mattiussi, and P. Berini,"Demonstration of intergrated optics elements based on long-ranging surface plasmon polaritons," Opt. Express **13**, 977–984 (2005).
4. J. Slavik and J. Homola, "Ultrahigh resolution long range surface plasmon-based sensor," Sens. Actuators B **123**, 10–12 (2007).
5. H. Raether, *Surface Plasmoncs on Smooth and Rough Surfaces and on Gratings* (Springer-Verlag, Berlin, 1988).
6. A.-L. Baudrion, F. de León-Pérez, O. Mahboub, A. Hohenau, H. Ditlbacher, F. J. García-Vidal, J. Dintinger, T. W. Ebbesen, L. Martín-Moreno, and J. R. Krenn, "Coupling efficiency of light to surface plasmon polariton for single subwavelength holes in a gold film," Opt. Express **16**, 3420–3429 (2008).
7. Y. Xie, A. Zakharian, J. Moloney, and M. Mansuripur, "Transmission of light through slit apertures in metallic films," Opt. Express **12**, 6106–6121 (2004).
8. H. J. Lezec and T. Thio, "Diffracted evanescent wave model for enhanced and suppressed optical transmission through subwavelength hole arrays," Opt. Express **12**, 3629–3651 (2004).
9. P. Lalanne, J. P. Hugonin, and J. C. Rodier, "Theory of surface plasmon generation at nanoslit apertures," Phys. Rev. Lett. **95**, 263902 (2005).
10. J. Wuenschell and H. K. Kim, "Surface plasmon dynamics in an isolated metallic nanoslit," Opt. Express **14**, 10000–10013 (2006).

#130935 - $15.00 USD Received 30 Jun 2010; revised 3 Aug 2010; accepted 3 Aug 2010; published 9 Aug 2010

11. L. Aigouy, P. Lalanne, H. Liu, G. Juli, V. Mathet, and M. Mortier, "Near-field scattered by a single nanoslit in a metal film," Appl. Opt. **46**, 8573–8577 (2007).
12. H. W. Kim, K. G. Lee, D. S. Kim, J. H. Kang, and Q.-H. Park, "Control of surface plasmon generation efficiency by slit-wdth tuning," Appl. Phys. Lett. **92**, 051115 (2008).
13. B. Wang, L. Aigouy, E. Bourhis, J. Gierak, J. P. Hugonin, and P. Lalanne, "Efficient generation of surface plasmon by single-nanoslit illumination under highly oblique incidence," Appl. Phys. Lett. **94**, 011114 (2009).
14. M. W. Kowarz, "Homogeneous and evanescent contributions in scalar near-field diffraction," Appl. Opt. **34** 3055–3063 (1995).
15. E. Palik, ed., *Handbook of Optical Constants of Solids* (Academic, 1998).

1. Introduction

Surface plasmon polaritons (SPPs) are bounded, transverse-magnetic (TM)-polarized electromagnetic modes that propagate along the interface between a dielectric and a metal and are confined to the interface by the exponential decay of the fields in the directions perpendicular to the interface. For frequencies above the near-infrared, the SPP wavelength can be significantly smaller than the wavelength of unbounded plane waves in the dielectric region. The field confinement and wavelength reduction achievable with SPPs hold promise to enabling dramatic miniaturization of the feature sizes of conventional optical devices [1–3] and optical sensors [4]. Due to the lack of widespread SPP sources, SPP devices typically incorporate a coupling structure to enable plane-wave modes to excite SPP modes [5]. Inefficiency associated with coupling from plane-wave modes into SPP modes remains a significant source of loss in SPP devices. Designing high-efficiency SPP coupling schemes remains an important objective in the efforts to enable real-world applications of SPPs [6].

Plane-wave illumination of a dielectric/metal interface does not enable coupling of plane-wave modes into SPP modes since the SPP wavevector does not intercept the plane-wave wavevector. Scatterers have been used to bridge the inherent wavevector mismatch between plane-wave and SPP modes. When a scatterer is illuminated, enhancement of the incident plane-wave wavevector by the Fourier components of the defect geometry enables wavevector matching between the incident light and the SPP mode. One of the most widely used techniques for SPP coupling is a single slit in a metal film [7–12]. A single slit is compact, amenable to integration, and insensitive to the incident angle of light. However, slit-coupling to SPP modes is inherently inefficient because a large fraction of the light incident on the slit is lost to radiation [8]. The motivation of this work is to devise a simple method to enhance the efficiency of SPP coupling at the exit of a slit via *dispersion engineering*, whereby the dielectric environment of the slit is modified to enable wavevector matching between the light emanating from the slit exit and the SPP mode on the adjacent metal surface.

2. Single-Slit SPP-Coupling Mechanism

Figure 1(a) depicts the geometry to be studied. A semi-infinite metal with relative permittivity ε_m is immersed in a dielectric medium with relative permittivity ε_d. The film extends infinitely in the x- and y-directions and occupies the region $-t < z < 0$. A slit of width w oriented parallel to the z-axis and centred at $y = 0$ is cut into the metal film. A transverse-magnetic (TM) polarized electromagnetic plane wave of wavelength λ_0 and wavevector $\sqrt{\varepsilon_d}k_0$, where $k_0 = 2\pi/\lambda_0$ is the free-space wavevector, is normally incident onto the bottom surface of the film located at $z = -t$. A fraction of the electromagnetic plane-wave mode incident onto the slit couples into a guided mode in the slit. Light exiting the slit in the region $z > 0$ consists of radiating and evanescent modes with wavevector magnitude $k_i \simeq \sqrt{\varepsilon_d}k_0$; coupling to the SPP mode on the metal surface is inefficient because k_i is less than the wavevector of the SPP mode on the metal

#130935 - $15.00 USD Received 30 Jun 2010; revised 3 Aug 2010; accepted 3 Aug 2010; published 9 Aug 2010

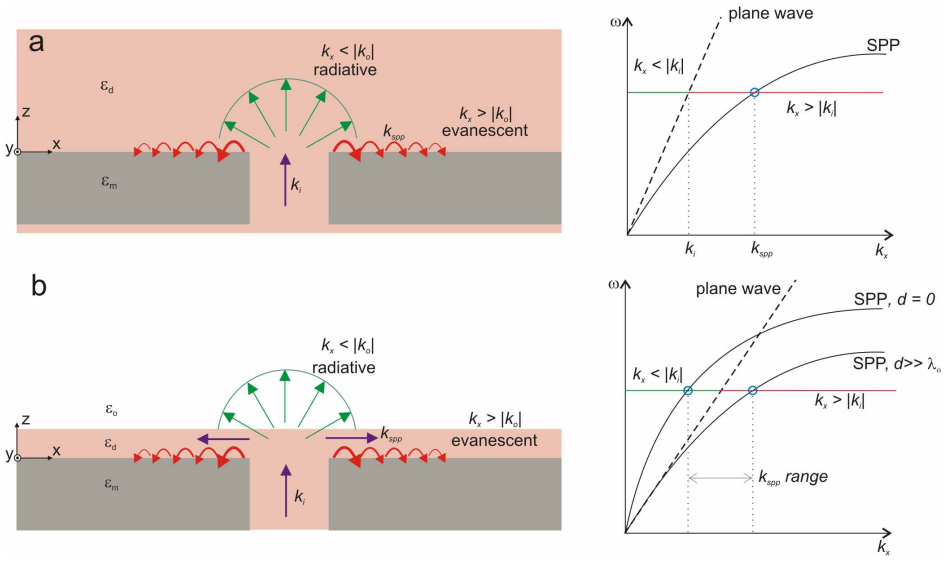

Fig. 1. (a) Real-space (left) and k-space (right) depictions of the modes scattering from the exit of a slit in a metal film when the metal film is completely immersed in a dielectric. (b) Real-space (left) and k-space (right) depictions of the modes scattering from the exit of a slit in a metal film when the slit is filled with a dielectric and the metal film is coated with a dielectric layer.

surface, k_{SPP}, given by

$$k_{SPP} = k_0 \left(\frac{\varepsilon_m \varepsilon_d}{\varepsilon_m + \varepsilon_d} \right)^{1/2}. \tag{1}$$

Diffraction at the slit exit disperses the modes at the slit exit into a continuum of directions described by $\vec{k} = k_x \hat{x} + k_z \hat{z}$. Assuming that the field at the exit of the slit in the plane $z = 0$ has the form

$$E(x,0) = \begin{cases} E_i & |x| < w/2 \\ 0 & |x| > w/2 \end{cases} \tag{2}$$

where E_i is a constant, the amplitude distribution of the diffraction spectrum is given by

$$A(k_x) = \frac{E_i}{\pi} \frac{\sin(k_x w/2)}{k_x}. \tag{3}$$

Diffracted modes that assume a real wavevector x-component $k_x < k_i$ possess a real wavevector z-component

$$k_z = \left(k_i^2 - k_x^2\right)^{1/2}, \tag{4}$$

corresponding to radiative modes that propagate away from the slit exit. On the other hand, diffracted modes that assume a real wavevector x-component $k_x > k_i$ possess an imaginary wavevector z-component

$$k_z = i\left(k_x^2 - k_i^2\right)^{1/2}, \tag{5}$$

corresponding to evanescent modes confined to the slit region. A fraction of the evanescent modes with values of k_x matching the wavevector of the SPP mode on the air-silver interface couple from the slit exit to the $\pm x$-directed SPP modes.

#130935 - $15.00 USD Received 30 Jun 2010; revised 3 Aug 2010; accepted 3 Aug 2010; published 9 Aug 2010

The total intensity radiated from the slit, I_r, is obtained by a summation, weighted by the squared amplitude distribution of the diffraction spectrum, of the intensities of the radiated modes [14]

$$I_r = \frac{4|E_i|^2}{\pi k w^2} \int_0^{k_i} \frac{\sin^2(kw/2)}{k^2} dk \tag{6}$$

Likewise, the total intensity confined to the slit-exit plane, I_e, is obtained by a summation of the intensities of the evanescent modes

$$I_e = \frac{4|E_i|^2}{\pi k w^2} \int_{k_i}^{\infty} \frac{\sin^2(kw/2)}{k^2} e^{-2\sqrt{k_x^2 - k_i^2} z} dk. \tag{7}$$

A fraction of I_e constitutes the SPP mode intensity I_{SPP} and the remainder constitutes the intensity of decaying modes I_d. The observable coupling efficiency of the radiating light from the slit to the SPP mode on the metal surface can be expressed as

$$\eta = \frac{I_{SPP}}{I_r + I_{SPP}}, \tag{8}$$

which assumes a value in the range $0 \leq \eta \leq 1$.

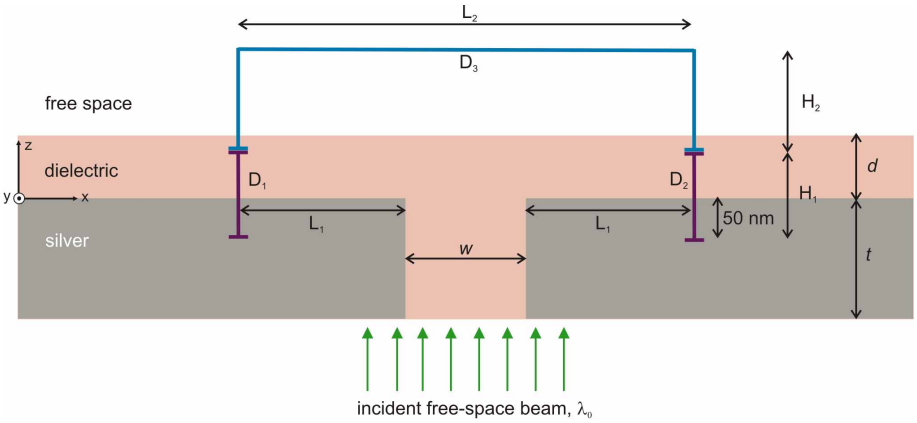

Fig. 2. Simulation geometry used to study SPP coupling from an illuminated slit. The detectors D_1 and D_2 capture the SPP modes, and the detector D_3 captures the radiating modes.

To enhance the SPP coupling efficiency from a slit, the configuration depicted in Figure 1(b) is proposed. A semi-infinite metal film with a slit of width w is immersed in free-space with permittivity ε_0. The slit in the film is completely filled with a lossless dielectric of relative permittivity ε_d. A semi-infinite dielectric layer, also of relative permittivity ε_d, is placed on the metal film such that it occupies the region $0 < z < d$. In the limits where $d \to \infty$ and $d \to 0$, the SPP wavevector approaches

$$k_{SPP} = k_0 \left(\frac{\varepsilon_m \varepsilon_d}{\varepsilon_m + \varepsilon_d} \right)^{1/2} \tag{9}$$

and

$$k_{SPP} = k_0 \left(\frac{\varepsilon_m}{\varepsilon_m + 1} \right)^{1/2}, \tag{10}$$

respectively. We assume that the magnitude of the wavevector of the radiating and evanescent modes at the slit exit in the region $z > 0$ is $k_i \simeq \sqrt{\varepsilon_d} k_0$; in reality, the light radiating from the

#130935 - $15.00 USD Received 30 Jun 2010; revised 3 Aug 2010; accepted 3 Aug 2010; published 9 Aug 2010

slit consists of a distribution of wavevector magnitudes, of which a large fraction corresponds to $\sqrt{\varepsilon_d}k_0$ [8, 14]. By varying the thickness of the dielectric layer, d, the effective wavevector of the SPP mode can be tuned such that $k_{SPP} \simeq k_i$, enabling efficient coupling of light from the slit into the SPP mode on the adjacent metal surface. The dielectric layer has an added practical benefit of passivation of the underlying metal surface; this is especially important for the case of silver, which tarnishes readily in the presence of atmospheric sulphur. To characterize this coupling scheme, we study the SPP-coupling efficiency as a function of the slit width ranging from 50 nm to 300 nm, the thickness of the dielectric layer ranging from 0 nm to 700 nm, and the wavelength ranging from 400 nm to 700 nm to determine a set of optimal parameters that yield maximum coupling. Judicious selection of the dielectric layer thickness and the slit width is shown to yield coupling efficiency $\eta \simeq 0.77$ extending over the visible wavelength range $400\,\text{nm} \leq \lambda_0 \leq 700\,\text{nm}$; the achieved efficiency is $\simeq 4$ times more efficient than that observed for a slit without the dielectric layer. Design guidelines are established to assist the experimentalist in realizing coupling geometries that yield optimal SPP coupling.

3. Methodology

We select numerical solutions of Maxwell's Equations via the finite-difference time-domain (FDTD) method to model the electromagnetic response of the isolated slit structure to quasi-plane-wave illumination conditions. The simulation grid has dimensions of 4000×1400 pixels with a resolution of 1 nm/pixel and is surrounded by a perfectly-matched layer to eliminate reflections from the edges of the simulation space. The structure consists of a 300-nm-thick silver film with a slit of width w; the dielectric in the slit and the dielectric layer on the metal film consist of dispersion-less glass with refractive index $\sqrt{\varepsilon_d} = 1.5$. The permittivity of silver is modeled by fitting to experimental data [15]. The corners of the slit are chamfered with a chamfer radius of 3 nm. This was done to eliminate perfectly sharp edges of the slit which can result in highly localized electric dipoles that affect the slit throughput [7]. The incident beam is centered in the simulation space at $x = 0$ and propagates in the $+z$-direction, with a full-width-at-half-maximum of 1200 nm and a waist located at $z = 0$. The incident electromagnetic wave has a wavelength 500 nm and is TM-polarized such that the magnetic field, H_y, is aligned along the y-direction.

The control variables are the incident polarization (TM), the metal type (silver), the dielectric type (dispersion-less glass), and the thickness of the metal layer ($t = 300\,\text{nm}$). The independent variables are the slit width w, which is varied from 50 nm to 300 nm in increments of 50 nm, the dielectric layer thickness d, which is varied from 0 nm to 700 nm in increments of 50 nm, and the free-space wavelength λ_0, which is varied over the visible frequency regime from 400 nm to 700 nm in increments of 100 nm. The dependent variables are the intensity of the SPP modes coupled to the exit surface of the metal film, I_{SPP}, the intensity of the radiated modes leaving the slit region, I_r, and the SPP coupling efficiency, η.

The dependent variables are quantified by placing line detectors, D_1, D_2, and D_3, in the simulation space to integrate the instantaneous magnitude squared of the magnetic field crossing the plane of the detectors (Figure 2). The detectors, D_1, D_2, and D_3, capture different components of the intensity pattern radiated from the exit of the slit. The line detectors D_1 and D_2 straddle the metal/dielectric interface and are situated adjacent to the slit exit a length $L_1 = \lambda_0$ away from the edges of the slit. D_1 and D_2 have identical heights $H_1 = \lambda_0/4 + 50\,\text{nm}$, of which 50 nm extends into the metal and $\lambda_0/4$ nm extends into the dielectric region above the metal. D_1 and D_2 capture the intensity of the left- and right-propagating SPP modes that are coupled from the slit and flow on the metal surface. The line detector D_3 is centered on the slit and extends over the dielectric region above the metal surface with a height of $H_2 = 3\lambda_0/4$ and a length of $L_2 = 2\lambda_0 + w$. D_3 captures the intensity of light radiated away from the slit that is not coupled

#130935 - $15.00 USD Received 30 Jun 2010; revised 3 Aug 2010; accepted 3 Aug 2010; published 9 Aug 2010

to the surface of the metal.

Because the detectors indiscriminately capture the intensity crossing the detector plane, I_r captured by D_1 and D_2 and I_{SPP} captured by D_3 constitute sources of error. The fraction of I_r captured by D_1 and D_2 is estimated by calculating the acceptance angle formed by the line detectors D_1 and D_2 with respect to the exit of the slit and integrating Eqn. 6 over this angle. At $\lambda_0 = 500\,\text{nm}$, $< 3\%$ of I_r is captured by D_1 and D_2. The fraction of I_{SPP} captured by D_3 is estimated from the attenuation of the SPP fields in the z-direction. At $\lambda_0 = 500\,\text{nm}$, $< 8\%$ of I_{SPP} is captured by D_3.

The time-averaged intensities of the SPP mode and the radiated modes are quantified by

$$I_{SPP} = \left\langle \int_{D_1} |H_y|^2 d\ell + \int_{D_2} |H_y|^2 d\ell \right\rangle \tag{11}$$

and

$$I_r = \left\langle \int_{D_3} |H_y|^2 d\ell \right\rangle \tag{12}$$

where the angled brackets indicate time-averaging of the quantity within the brackets.

4. Control Studies

Table 1. Control simulation geometries and results. Fixed parameters include $w = 150\,\text{nm}$, $d = 100\,\text{nm}$, $t = 300\,\text{nm}$, and $\lambda_0 = 500\,\text{nm}$

Simulation Geometry	λ_i	λ_{SPP}	η
	500 nm	473 nm	20%
	500 nm	473 nm	21%
	333 nm	292 nm	25%

Three control simulations are performed to establish baseline SPP-coupling-efficiency values. The control structures consists of a silver film of thickness $t = 300\,\text{nm}$ having a slit width of $w = 150\,\text{nm}$, where (1) the film is surrounded by free space and the slit is filled with free space, (2) the film is surrounded by free space and the slit is filled with glass, and (3) the film is surrounded by free-space and the slit is filled with glass. The slits are illuminated with a quasi-plane wave with a wavelength $\lambda_0 = 500\,\text{nm}$. Each geometry represents different situations in which the magnitude of the wavevector (or equivalently, wavelength) of the light radiating in the immediate vicinity of the slit exit is mismatched with the SPP wavevector (or wavelength) on the metal surface. The wavelength of the emanating light, λ_i, and of the SPP mode, λ_{SPP}, are given in Table 1.

#130935 - $15.00 USD Received 30 Jun 2010; revised 3 Aug 2010; accepted 3 Aug 2010; published 9 Aug 2010

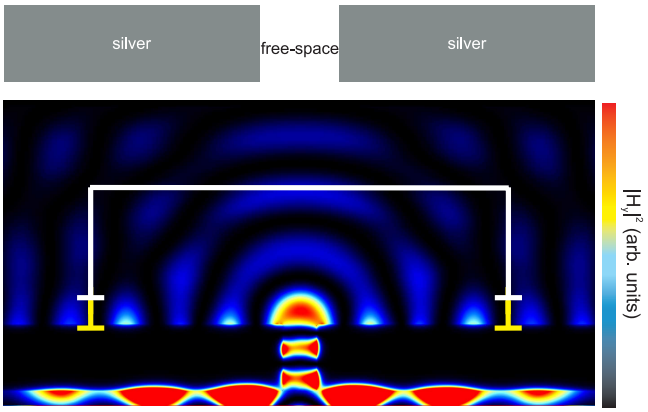

Fig. 3. Image of the FDTD-calculated instantaneous $|H_y|^2$ distribution for a slit of width $w = 150\,\text{nm}$ illuminated by a quasi-plane-wave of wavelength $\lambda_0 = 500\,\text{nm}$. The simulation geometry is depicted by the above graphic. Lines indicating the position of detectors D_1, D_2, and D_3 have been superimposed on the image.

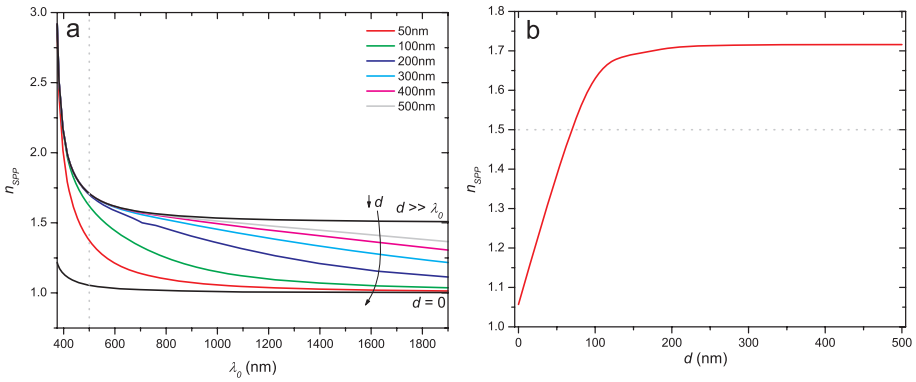

Fig. 4. Principle of dispersion engineering to enhance slit-coupling to SPP modes. (a) Dispersion curve of n_{SPP} as a function of λ_0 for various d calculated from the roots of the eigenvalue equation for the SPP mode on an asymmetric, three-layer silver-glass-air waveguide. (b) n_{SPP} as a function of d for $\lambda_0 = 500\,\text{nm}$. The dotted gray line corresponds to the refractive index of a plane-wave mode in glass, $\sqrt{\varepsilon_d}$.

5. Results and Discussion

Shown in Fig. 3 is a snap-shot of the instantaneous $|H_y|^2$ distribution for illumination of the silver film immersed in free space. The slit sustains a field-symmetric mode that carries electromagnetic energy across the extent of the slit. A significant portion of the fields radiating from the slit exit propagates in free-space away from the metal surface (captured by the D_3 detector), and a lesser portion of the fields couple into confined left- and right-propagating modes on the metal surface (captured by the detectors D_1 and D_2). The wavelength of the confined mode on the metal surface is $\lambda_{SPP} = 480 \pm 10\,\text{nm}$, where the error corresponds to the observed variation of the SPP mode wavelength as a function of distance from the slit. An SPP coupling efficiency of $\simeq 0.20$ is measured for the slit immersed in free space. SPP coupling efficiencies of $\simeq 0.21$

#130935 - $15.00 USD Received 30 Jun 2010; revised 3 Aug 2010; accepted 3 Aug 2010; published 9 Aug 2010

and $\simeq 0.25$ are measured, respectively, for the dielectric-filled slit immersed in free space and the slit immersed in dielectric (see Table 1).

Variations in the thickness of the dielectric layer on the metal film enable tuning of the SPP wavevector, k_{SPP}, and hence, the effective refractive index of the SPP mode, $n_{SPP} = k_{SPP}/k_0$. The dispersion curves for n_{SPP} as a function of λ_0 and d are determined by iteratively solving the complex eigenvalue equation for the wavevector k_{SPP} of the mode sustained by an asymmetric, three-layer silver-glass-air waveguide, where the thickness of the glass layer is d. As shown in Fig. 4(a), n_{SPP} increases asymptotically as λ_0 decreases from 1900 nm to 400 nm. For finite d, the n_{SPP} dispersion curves are bound between the curves corresponding to $d = 0$ (air-silver interface) and $d >> \lambda_0$ (glass-silver interface). As shown in Fig. 4(b), at a fixed $\lambda_0 = 500$ nm, n_{SPP} as a function of d can assume a continuum of values in the range $1.05 < n_{SPP} < 1.72$. The condition $n_{SPP} \simeq \sqrt{\varepsilon_d} = 1.5$ is predicted to occur for a dielectric layer thickness $d \simeq 75$ nm.

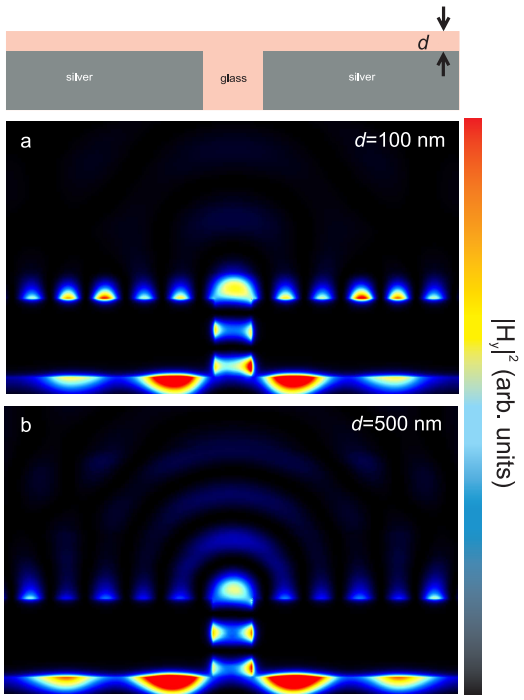

Fig. 5. Image of the FDTD-calculated instantaneous $|H_y|^2$ distribution for a slit of width $w = 150$ nm illuminated by a quasi-plane-wave of wavelength $\lambda_0 = 500$ nm when a dielectric layer of thickness (a) 100 nm and (b) 500 nm is placed on the metal film. The simulation geometry is depicted by the above graphic.

Figure 5 displays the instantaneous $|H_y|^2$ distributions for illumination of silver films with dielectric layer thicknesses of $d = 100$ nm and $d = 500$ nm. The slit width $w = 150$ nm is held constant. High-efficiency SPP coupling is evident for $d = 100$ nm; the presence of the $d = 100$ nm dielectric layer on the metal film yields negligible radiated intensity and relatively high SPP intensity. SPP coupling efficiency drops as the dielectric layer thickness increases to $d = 500$ nm; the $|H_y|^2$ distribution reveals an increase in the radiated intensity and a reduction in the SPP intensity relative to that for $d = 100$ nm.

Figure 6 displays the time-averaged radiated intensity I_r and time-averaged SPP intensity I_{SPP} as a function of d, along with the corresponding SPP-coupling efficiency, η. Appropri-

#130935 - $15.00 USD Received 30 Jun 2010; revised 3 Aug 2010; accepted 3 Aug 2010; published 9 Aug 2010

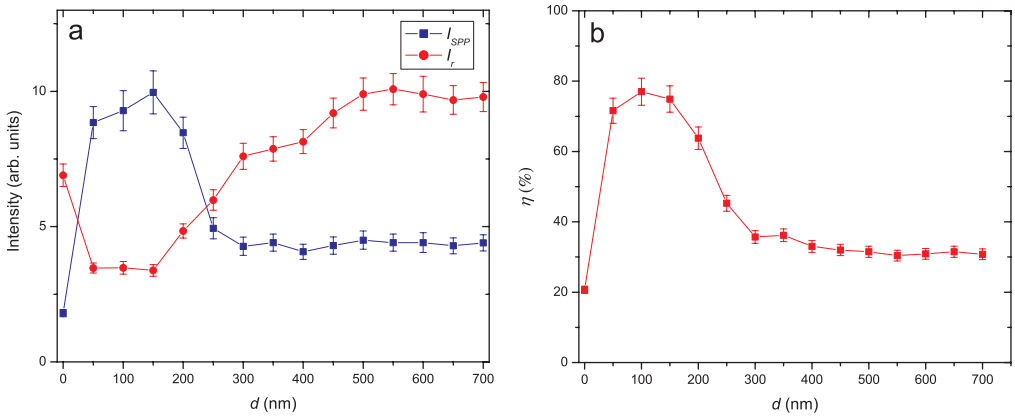

Fig. 6. (a) The time-averaged SPP intensity, I_{SPP} (blue squares), and time-averaged radiated intensity, I_r (red circles), and (b) the corresponding SPP coupling efficiency, η, as a function of d. The error bars describe the uncertainties in the measurement of I_{SPP} and I_r due to, respectively, the finite amount of I_r captured by D_1 and D_2 and the finite amount of I_{SPP} captured by D_3.

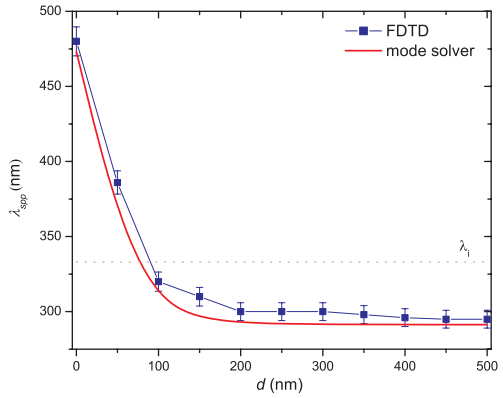

Fig. 7. SPP wavelength measured from the FDTD simulations (blue squares) and predicted from the mode solver (red line) as a function of dielectric layer thickness d. The dotted gray line indicates the value of $\lambda_i = \lambda_0/\sqrt{\varepsilon_d}$. The error bars describe the uncertainty in the measurement of λ_{SPP} from the FDTD simulations due to variation in λ_{SPP} as a function of distance from the slit exit.

ately selecting the dielectric layer thickness can yield both enhanced SPP coupling and reduced radiation from the slit. For values of d in the range $50\,\text{nm} < d < 150\,\text{nm}$, I_{SPP} is near-maximum and I_r is near-minimum, yielding an SPP-coupling efficiency $\simeq 0.77$. For values of $d > 150\,\text{nm}$, the efficiency curve drops and flattens. In the limits where $d \to 0\,\text{nm}$ and $d \to 700\,\text{nm}$, the SPP-coupling efficiencies approach $\eta \to 0.20$ and $\eta \to 0.31$, respectively.

The layer thickness corresponding to high coupling efficiency approximately coincides with the layer thickness where the SPP wavelength, λ_{SPP}, matches the wavelength of light at the slit exit $\lambda_i = \lambda_0/\sqrt{\varepsilon_d}$. Figure 7 plots the SPP wavelength as a function of the dielectric layer thickness d. The SPP wavelength has been obtained by two methods: direct measurement from the FDTD-calculated $|H_y^2|$ distributions and calculation via the SPP modal solutions of the

#130935 - $15.00 USD Received 30 Jun 2010; revised 3 Aug 2010; accepted 3 Aug 2010; published 9 Aug 2010

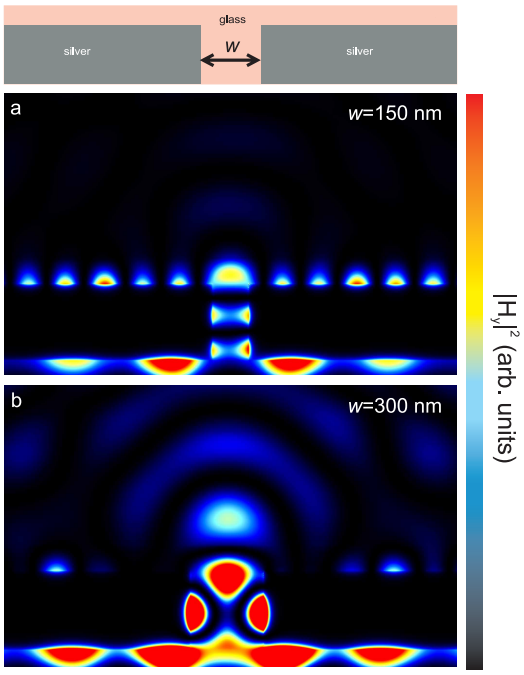

Fig. 8. Image of the FDTD-calculated instantaneous $|H_y|^2$ distribution for a slit illuminated by a quasi-plane-wave of wavelength $\lambda_0 = 500\,\text{nm}$ when the slit width is (a) 150 nm and (b) 300 nm. The dielectric layer thickness $d = 100\,\text{nm}$ is held constant. The simulation geometry is depicted by the above graphic.

asymmetric silver-glass-air waveguide. There is a good match between the SPP wavelength values obtained by the FDTD simulations and the modal solutions. As d increases from 0 nm to 500 nm, the SPP wavelength reduces from 480 nm to 300 nm. At the layer thickness $d \simeq 100\,\text{nm}$ yielding maximum SPP coupling efficiency, k_{SPP} nearly matches k_i, which has been assumed to be $\sqrt{\varepsilon_d}k_0$ (although this is not generally true, as the modes at the exit of the slit assume a distribution of wavevector magnitudes). The correlation between the high coupling efficiency and wavelength similarity between the SPP mode and the plane-wave mode in the dielectric suggest that phase-matched coupling is the primary culprit in the efficiency enhancement.

Changing the slit width affects the distribution of the modes at the exit of the slit, which in turn affects the SPP coupling efficiency. Figure 8 displays the instantaneous $|H_y|^2$ distributions for illumination of silver films with slit widths of $w = 150\,\text{nm}$ and $w = 300\,\text{nm}$. The dielectric layer thickness $d = 100\,\text{nm}$ is held constant. The narrower slit shows weaker overall transmission through the slit, with the majority of the transmitted field coupled into the bounded SPP modes on the metal surface at the exit side of the slit. The wider slit exhibits greater overall transmission, with a significant portion of the transmission radiating from the metal surface. As w increases, a greater percentage of the modes at the slit exit are propagating modes that radiate away from the metal surface. In the limit where the slit width is very large ($w >> \lambda_0$), a ray picture can be used where the majority of the incident light rays propagate directly through the slit and away from the slit exit.

Increasing the slit width generally reduces the efficiency of SPP coupling from the slit structure. The influence of the slit width on I_{SPP}, I_r, and η is plotted in Fig. 9. As w increases from 50 nm to 300 nm, I_r increases monotonically, while I_{SPP} peaks at $w = 250\,\text{nm}$ and then

#130935 - $15.00 USD Received 30 Jun 2010; revised 3 Aug 2010; accepted 3 Aug 2010; published 9 Aug 2010

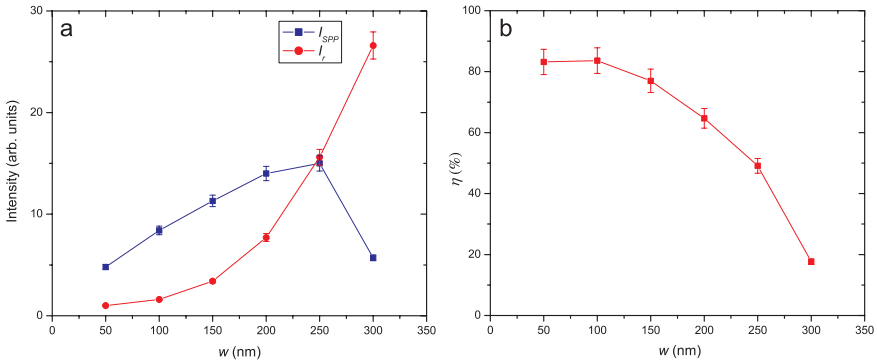

Fig. 9. a) The time-averaged SPP intensity, I_{SPP} (blue squares), and time-averaged radiated intensity, I_r (red circles), and (b) the corresponding SPP coupling efficiency, η, as a function of w. The error bars describe the uncertainties in the measurement of I_{SPP} and I_r due to, respectively, the finite amount of I_r captured by D_1 and D_2 and the finite amount of I_{SPP} captured by D_3.

decreases at $w = 300$ nm. The corresponding SPP coupling efficiency monotonically decreases from $\simeq 0.83$ to $\simeq 0.18$ as the slit width increases from 50 nm to 300 nm.

To investigate the wavelength-sensitivity of the coupling structure, the electromagnetic response of a coupling structure with slit width $w = 200$ nm and dielectric layer thickness $d = 100$ nm is studied over free-space wavelengths ranging from 400 nm to 700 nm, in increments of 100 nm. SPP- coupling efficiencies of 0.66, 0.67, 0.66, and 0.65 are observed at wavelengths of 400 nm, 500 nm, 600 nm, and 700 nm, respectively. The coupling efficiency is largely insensitive to wavelength because the condition $k_{SPP} \simeq k_i$ is achieved via near-field perturbation of the SPP mode using a $d << \lambda_0$ layer. That is, the dielectric layer shifts the k_{SPP} wavevector commensurately throughout the visible frequency range.

6. Summary

In conclusion, we have proposed a method for enhancing the efficiency of slit-coupling from a free-space plane-wave mode into a SPP mode on a metal film. The key element of the coupling scheme involves an ultra-thin dielectric layer placed on the exit side of the metal film. Varying the thickness of the dielectric layer enables tuning of the SPP wavevector. When the SPP wavevector is matched with the wavevector magnitude of the modes exiting the slit, coupling efficiencies $\simeq 0.80$ can be achieved, $\simeq$ 4-times enhancement relative to the case without the dielectric layer. In addition to enhancing SPP coupling efficiency, the dielectric layer has the added benefit of passivation and protection of the SPP-sustaining metal surface. The results will find utility in the growing field of plasmonics and help pave the way towards real-world implementation of SPP devices.

Acknowledgements

The authors thank H. Lezec for helpful discussions. This work was supported by the Natural Sciences and Engineering Research Council of Canada.

#130935 - $15.00 USD Received 30 Jun 2010; revised 3 Aug 2010; accepted 3 Aug 2010; published 9 Aug 2010